

Advanced Reactor Safeguards

# ***Assessment of Flow-Enhanced Electrochemical Sensor Testing and Deployments for MSRs***

Prepared for  
US Department of Energy

Colin E. Moore, William H. Doniger, and Nathaniel C. Hoyt  
Argonne National Laboratory

September 30, 2023  
ANL/CFCT-23/38

*[This page intentionally left blank]*

## ABSTRACT

This report serves as the deliverable for Milestone M3RS-23AN0401061 that is part of Work Package RS-23AN040106 (Flow Enhanced Sensors for MSRs – ANL). The goal of this milestone was to determine performance of the flow enhanced electrochemical sensor (FEES) and modular flow instrumentation testbed (MFIT) in safeguards relevant scenarios. Flow enhanced electrochemical sensors are a type of electroanalytical sensor that has been developed at Argonne National Laboratory to be installed directly into MSR flow conduits to make measurements of the salt composition. These sensors represent a significant improvement in capabilities compared to earlier electroanalytical sensors that instead can only be operated in quiescent conditions. Previous work has focused on testing of the FEES in flowing conditions provided by the MFIT to assess the accuracy and precision of the sensor measurements. To further improve this capability, in FY23 we undertook a campaign of safeguards relevant scenarios in molten salt containing a range of uranium chloride concentrations (0 to 3 wt%). All the testing carried out in FY23 was aided by a control system designed to automatically actuate flow conditions and collect data. This new automation system is estimated to have increased experimental throughput by a factor of four and enabled testing in a variety of complex conditions. The advancements in throughput and repeatability led to improved quantification of actinide concentrations using the in-flow sensors, with a reduction of the mean absolute relative error from 5.6% in FY22 to 3.1% in FY23.

In addition to safeguards scenarios run in the MFIT, FY23 work included deployment of a FEES at a partner institution where it will be tested in a flowing salt loop. The FEES was successfully integrated into that loop and is being tested prior to loop startup. In FY23, work also continued on the smaller flow system that we have named the mini-MFIT. This smaller system is capable of rapid prototyping of new sensor designs prior to installation in the larger MFIT radiological flow system. Work was carried out to test this new system in non-radiological molten salts in a separate glovebox. This work is helping us to enhance the accuracy of our salt monitoring capabilities through the integration of multiple types of sensors. The high degree of accuracy required by 10 CFR 74 represents a significant challenge, and further design evolution and integration of the sensors into multimodal sensing frameworks will be needed to further push the measurement accuracy to the needed level.

## CONTENTS

	ABSTRACT .....	iii
	CONTENTS .....	iv
	FIGURES .....	v
	ACRONYMS AND ABBREVIATIONS .....	vi
	ACKNOWLEDGEMENTS .....	vii
1.	INTRODUCTION .....	1
2.	EXPERIMENTAL SETUP .....	2
2.1	MFIT System overview .....	2
2.2	MFIT Fuel Salt Preparation .....	4
2.3	Mini-MFIT System Overview.....	5
2.4	Mini-MFIT Operations .....	5
2.5	Mini-MFIT Salt Tank Level Sensor.....	7
2.6	Software for Process Control and FEES Sensor Automation .....	8
2.7	Mini-MFIT Shakedown Testing Using NaCl-KCl-MgCl <sub>2</sub> Salt .....	9
3.	RESULTS.....	11
3.1	Automated Transfers.....	11
3.2	Sensor Assessment Campaign.....	11
4.	Engineering-Scale FEES Sensor Deployment.....	16
5.	CONCLUSIONS .....	17
	REFERENCES.....	18

## FIGURES

<b>Figure 1.</b> Pictures of (a) MFIT complete with heater assemblies, sensors and insulation installed into an (b) inert atmosphere glovebox. ....	3
<b>Figure 2.</b> $\text{UCl}_3$ -NaCl production. (a) DU dendrites from electrorefining operations, (b) $\text{UCl}_3$ after distillation and (c) $\text{UCl}_3$ inside of stainless-steel crucible prior to closing MFIT pressure vessel. ....	4
<b>Figure 3.</b> Mini-MFIT (a) rendering and (b) assembly without the furnace lid and (c) schematic of sensors and fluid flow path. ....	5
<b>Figure 4.</b> Gas control system (left) and Mini-MFIT system (right) installed in a non-radiological glovebox. ....	6
<b>Figure 5.</b> FEES sensor signal during a single Mini-MFIT fill and drain cycle. Constant potential measurements at 0.5 V vs. W quasi-reference electrode in NaCl-KCl-MgCl <sub>2</sub> at 500 °C. Mass flow rate during filling step equals 0.9 SLPM. ....	7
<b>Figure 6.</b> Mini-MFIT salt level sensor (a) continuity measurement device, (b) electrode array sensor, and (c) diagram of salt level sensor placement in the MINI-MFIT salt tank. ....	8
<b>Figure 7.</b> Mini-MFIT salt tank level sensor digital indicator software. ....	8
<b>Figure 8.</b> MFIT control software for process automation and FEES sensor control. ....	9
<b>Figure 9.</b> Mini-MFIT argon gas mass flow rate versus time for a repeated sequence of cycles at various set-points during testing in NaCl-KCl-MgCl <sub>2</sub> at 500 °C. ....	9
<b>Figure 10.</b> Mini-MFIT constant potential measurements during flow cycles at different mass flow controller setpoints in NaCl-KCl-MgCl <sub>2</sub> at 500 °C. The applied potential equals 0.5 V vs. W quasi-reference electrode. ....	10
<b>Figure 11.</b> (a) Concentration calculation from FEES during 80 transfers at $4.38 \pm 0.12$ L/min in MgCl <sub>2</sub> -KCl-NaCl containing 2.0 wt% $\text{UCl}_3$ . (b) Current response of FEES during 80 transfers. ....	11
<b>Figure 12.</b> Concentration determined using stationary salt sensor in (MAVS) measured in MgCl <sub>2</sub> -KCl-NaCl- $\text{UCl}_3$ . ....	12
<b>Figure 13.</b> Current response of flow sensor at different $\text{UCl}_3$ concentrations. Measurements were taken approximately 4.5 SLPM salt flow rate. ....	12
<b>Figure 14.</b> $\text{U}^{3+}/\text{U}^{4+}$ current response and histograms of 10 repeat transfers using the FEES. ....	13
<b>Figure 15.</b> Experimentally measured current response of flow sensor at different $\text{U}^{3+}$ concentrations and flow rates. Lines represent the nonlinear-surface fit for the sensor response function. ....	14
<b>Figure 16.</b> Parity plot of uranium concentration from process knowledge and uranium concentration measured using the FEES. ....	15
<b>Figure 17.</b> FEES sensors deployed at industrial partner’s engineering scale forced convection FLiBe experiment. ....	16
<b>Figure 18.</b> FEES sensor installed in industrial partner’s flow loop ....	16

## ACRONYMS AND ABBREVIATIONS

ANL	Argonne National Laboratory
CA	Chronoamperometry
CV	Cyclic Voltammogram
DOE	US Department of Energy
EIS	Electrochemical Impedance Spectroscopy
FEES	Flow-Enhanced Electrochemical Sensor
FHR	Fluoride salt-cooled High-temperature Reactors
MAVS	Multielectrode Array Voltammetry Sensor
MC&A	Materials Control and Accounting
MFC	Mass Flow Controller
MFR	Measured Flow Rate
MFIT	Modular Flow Instrumentation Testbed
MSR	Molten Salt Reactor
PT	Pressure Transducer
SLPM	Standard Liters Per Minute
TC	Thermocouple

## **ACKNOWLEDGEMENTS**

This report was produced under the auspices of the US DOE Office of Nuclear Energy's Advanced Reactor Safeguards Program, Dr. B. Cipiti, National Technical Director and S. Fitzwater, Program Manager.

This work was conducted at Argonne National Laboratory and supported by the U.S. Department of Energy, Office of Nuclear Energy, under Contract DE-AC02-06CH11357.

Advanced Reactor Safeguards Program

# ASSESSMENT OF THE FLOW-ENHANCED SENSORS FOR ACTINIDE QUANTIFICATION IN MSRs

## 1. INTRODUCTION

In support of the Advanced Reactor Safeguards program, Argonne National Laboratory has developed advanced sensors and a modular flow instrumentation testbed (MFIT) applicable to liquid-fueled molten salt reactors (MSRs) and fluoride salt-cooled high-temperature reactors (FHRs). Several techniques have been suggested for material control and accountancy including dynamic modeling, [1, 2] in-line spectroscopic [3, 4] or electrochemical techniques, [5] and at-line destructive techniques. [6, 7] MSRs and FHRs create challenging conditions that make it difficult to design and operate sensors for long periods without failure of the sensing mechanism. Actinide quantification is an integral part of material control and accountancy regulations found in 10 CFR 74.

One of the most significant challenges with sensor operations in MSRs is the high flow velocities that are present within the reactor's primary and secondary fluid streams. These velocities can cause large distortions in measurements, particularly for electroanalytical sensors. As such, all of Argonne's sensor designs prior to this project have been designed to be installed in quiescent zones using shrouds or other isolation approaches. Although Argonne has successfully demonstrated the use of shrouded electrodes over long-durations in thermal convection loops with flowing molten salts, this approach does have drawbacks. For example, the shrouding slows the mass transport of species from the bulk, lowering the response time of the measurements. Additionally, the lack of flow only permits intermittent, dynamic electroanalytical techniques to be used (e.g., voltage sweeps) as opposed to potentiostatic and galvanostatic measurements that fare better with respect to the extreme electrical noise induced in a reactor environment. To address these issues, and provide optimized measurement capabilities that can meet challenging mass accountancy requirements, Argonne has developed flow-enhanced electrochemical sensors. The measurements from these sensors are based on the electrochemical response of electrodes immersed directly in the flow of the molten salt. To achieve flow conditions representative of molten salt reactor flow conditions, Argonne constructed a testbed for the operations of safeguards-relevant flow instrumentation. This system, known as the MFIT, can accommodate a wide variety of interchangeable sensor test sections to permit the testing of the sensors under a variety of conditions and configurations.

Initial molten salt operations with the MFIT began in FY21. FY22 saw the completion of a test campaign which identified electrochemical waveforms useful for the determination of actinide concentrations and molten salt flow rates. The goal of the FY23 work package was to improve the precision of the flow enhanced sensors and deploy one of the sensors at a partner institution. To further test the performance of these sensors, we also carried out a testing campaign using the established waveforms on safeguards relevant scenarios within the modular flow instrumentation testbed. Lessons learned from the previous testing campaign were applied to improve the chemical stability of the salt. Additionally, a newly designed and installed LabVIEW-based automation system markedly improved experimental throughput and data acquisition, allowing us to collect far more data than we had been able to in previous years.

This report summarizes the activities conducted during FY23. During this period, improvements to operations, sensor performance, and data analysis approaches were achieved. These combined activities are intended to help vendors achieve the regulatory requirements for material accountancy (10 CFR 74).



## 2. EXPERIMENTAL SETUP

Two experimental apparatus were constructed to support the development of the flow enhanced electrochemical sensor (FEES) and other safeguards-relevant sensors. Both systems are specifically designed for installation within a glovebox. These forced flow systems provide similar geometries for installation of FEES sensors but differ in the method of inducing flow. The Modular Flow Instrumentation Testbed (MFIT) uses a positive pressure differential to achieve high flow rates between 3 and 10 standard liters per minute (SLPM). It can also accommodate radiological materials, such as depleted uranium salts. The mini-MFIT is a scaled down version which utilizes a negative pressure differential to achieve flow rates less than 2 SLPM. The mini-MFIT leverages existing glovebox infrastructure and enables the salt composition to be more easily changed. This allows us to make rapid prototyping changes and resolve design questions effectively. These systems were designed with careful consideration for operations, and numerous safety devices including relief valves, gas cut-off valves, a pneumatically actuated pressure relief valve, and a bubbler are included in the final construction.

A variety of transfer line diameters can be accommodated to create conditions representative of sampling lines, bypass lines, or the main coolant conduits on an MSR. The experimental results for both MFIT systems in this report were conducted in a 0.5" diameter transfer tube.

Both MFIT systems have been successfully retrofitted with a process and instrumentation software aimed at increasing repeatability, throughput, and safety of MFIT and FEES sensor operation. These features have allowed us to make hundreds of salt transfers over the past year without any significant operational issues.

### 2.1 MFIT System overview

The MFIT (specifications in Table 1) consists of two pressure tanks connected by a molten salt transfer line (Figure 1a). A flow enhanced electrochemical sensor (FEES) is installed in the center of the transfer line. A multielectrode array voltammetric sensor (MAVS) is installed on the tank and makes measurements in the stationary salt to determine the uranium concentration. All electrochemical measurements were taken using a Gamry Interface 5000E potentiostat. The MFIT is installed in a glovebox (Figure 1b) which allows for large quantities of radiological salts to be used and enables rapid installation and modification of new sensor designs and configurations. Pressurized argon gas is used to create the forced-flow conditions within the MFIT (Figure 1a). This system was designed with careful consideration for operations, and numerous safety devices including relief valves, gas cut-off valves, a pneumatically actuated pressure relief valve, and a bubbler are included in the final construction. One issue that was seen during FY22 operations was an ingress of air into the transfer system. The argon handling system was upgraded, and leaks were repaired. This allowed us to make transfers without introducing any air or water vapor into the system. Doing so kept the speciation of the  $UCl_3$  consistent during testing and reduced inaccuracies in the results.

**Table 1.** MFIT specifications and capabilities

Modular Flow Instrumentation Testbed	
<b>Capacity</b>	Max 10 L (Currently operating with 2 L)
<b>Flow rate range</b>	0.5 to 50 L/min gas flow rate, 3 to 10 L/min salt flow rate
<b>Heaters</b>	6 heated zones, Max 650 °C 13,300 W
<b>Process sensors</b>	16 Thermocouples, 2 Pressure transducers
<b>Electrochemical sensors</b>	Stationary salt (MAVS), Flowing salt (FEES)
<b>Max pressure</b>	20 psi
<b>Expansion ports</b>	10 (5 on each tank) 0.25" to 1" in diameter

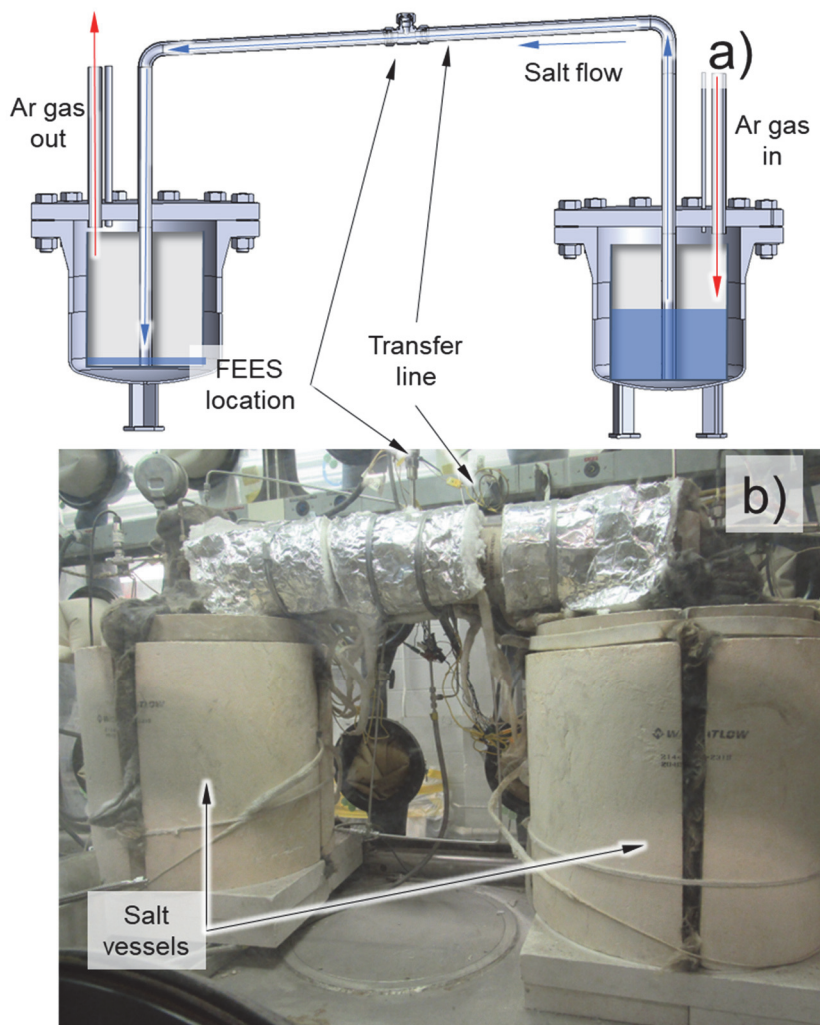


**Figure 1.** Pictures of (a) MFIT complete with heater assemblies, sensors and insulation installed into an (b) inert atmosphere glovebox.

## 2.2 MFIT Fuel Salt Preparation

Preparation for operations with  $\text{UCl}_3$ -bearing fuel salts were initiated in Q2 FY23. This work involved the production of several kilograms of  $\text{MgCl}_2$ - $\text{KCl}$ - $\text{NaCl}$ - $\text{UCl}_3$  salt. The same method as in FY22 was employed to produce 4 kg of salt purified salt. All  $\text{MgCl}_2$ - $\text{KCl}$ - $\text{NaCl}$  was again purified using Mg metal contacting to remove any corrosive species prior to placing into the MFIT. This process produces some  $\text{HCl}(\text{g})$  from impurities in the salt. The  $\text{HCl}$  was collected using an off-gas system which allows us to purify large batches of salt (2–5 kg) without damaging glovebox components. The  $\text{MgO}$  is insoluble in the salt and sinks to the bottom where it can be removed once the salt cools. After completing the purification procedure,  $\text{UCl}_3$  was added to the salt to bring the concentration to 0.5 wt%. Titration of the operating salt with  $\text{UCl}_3$  was carried out during the experimental campaign to bring the final concentration up to 3 wt% (FY22 concentrations stopped at 2 wt%) in increments of 0.5 wt%. Electrochemical measurements were taken at each interval.



**Figure 2.**  $\text{UCl}_3$ - $\text{NaCl}$  production. (a) DU dendrites from electrorefining operations, (b)  $\text{UCl}_3$  after distillation and (c)  $\text{UCl}_3$  inside of stainless-steel crucible prior to closing MFIT pressure vessel.

### 2.3 Mini-MFIT System Overview

The mini-MFIT was designed and constructed in FY22 to ensure that sufficient data would be generated to complete the FEES assessments. Like the larger MFIT, the mini-MFIT was designed for rapid, automated assessments of electrochemical sensors and investigation of flowing salt environments. The compact design was able to fit within an existing furnace well at Argonne to enable quick deployment. Pictured in Figure 3, the mini-MFIT flow system consists of a salt crucible, dip tube, salt tank, and gas control system. This system is suspended from the furnace lid with a gas control line and additional sensors penetrating through the well's heat shield assembly. A FEES was inserted into the flow path inside the dip tube. An additional level sensing electrochemical probe was inserted into the salt tank to monitor the level of the salt and provide an additional measurement of salt flow rate. An electrochemical crucible sensor has been added to measure salt properties in quiescent salt conditions for comparison to the flowing salt data. This flow system can accommodate a maximum of 500 mL of salt which can easily be replaced or modified during testing.

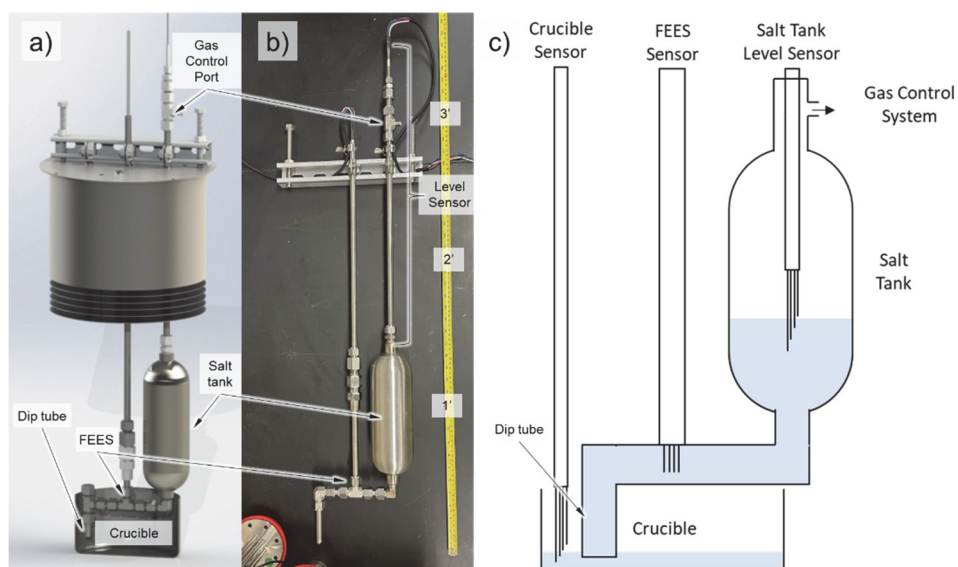


**Figure 3.** Mini-MFIT (a) rendering and (b) assembly without the furnace lid and (c) schematic of sensors and fluid flow path.

### 2.4 Mini-MFIT Operations

In early FY23, the mini-MFIT was installed in a non-radiological glovebox at Argonne. Figure 4 shows the mini-MFIT system suspended from the well furnace lid (right) and the gas control system (left). In Q1 FY23, shakedown testing was performed using 500 mL of magnesium contacted NaCl-KCl-MgCl<sub>2</sub> at 500 °C. The system was operated at temperature for one week and completed approximately 70 fill and drain cycles at flow rates up to 2 SPLM. Electrochemical experiments conducted with purified salt were useful for measuring sensor baseline behavior without the presence of dissolved analytes.

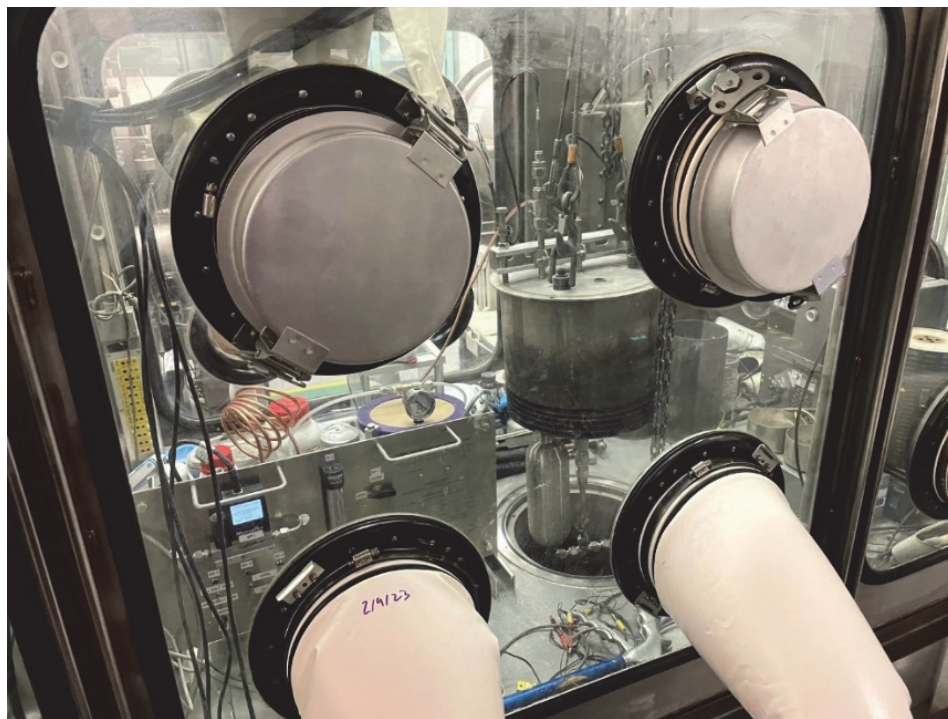


**Figure 4.** Gas control system (left) and Mini-MFIT system (right) installed in a non-radiological glovebox.

The Mini-MFIT FEES shakedown testing was conducted with a typical fill and drain cycle that included a 10 second hold, a 60 second fill, and a 20 second drain step. Figure 5 shows the current response from a FEES sensor operating in constant potential mode at 0.5 V vs. a W quasi-reference electrode in NaCl-KCl-MgCl<sub>2</sub> at 500 °C. While no dissolved species were intentionally added to the salt, it was assumed that the measured current correlated the oxidation of dissolved impurities, such as trace amounts of CrCl<sub>2</sub>. The constant potential data is well correlated with physical events in the mini-MFIT. During the hold step, application of the potential without salt flowing in the dip tube resulted in some initial current that decreased rapidly. This was assumed to be due to a thin film of salt present on the sensor from previous cycles. As the CrCl<sub>2</sub> in this film was quickly depleted the current fell to near zero, as expected. When the FEES sensor was fully submerged in salt, the current versus time was dictated by the mass transport of oxidizable impurities to the electrode surface. During the drain step, the salt was allowed to flow quickly back down into the crucible. The rush of salt past the FEES sensor caused a spike in current that then quickly decayed as the residual salt drained out of the dip tube.

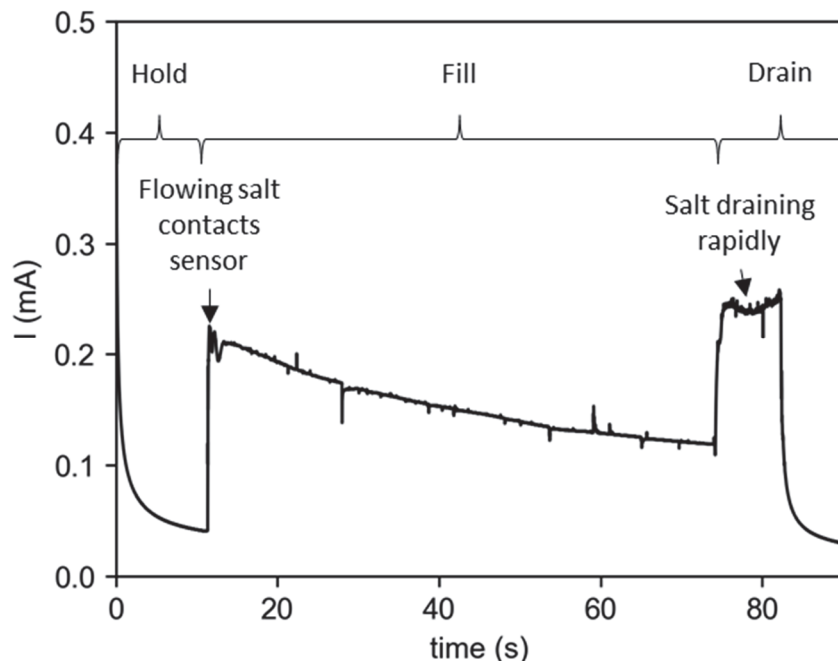


**Figure 5.** FEES sensor signal during a single Mini-MFIT fill and drain cycle. Constant potential measurements at 0.5 V vs. W quasi-reference electrode in NaCl-KCl-MgCl<sub>2</sub> at 500 °C. Mass flow rate during filling step equals 0.9 SLPM.

## 2.5 Mini-MFIT Salt Tank Level Sensor

In FY23, a new salt level sensor was designed and constructed for verification of fluid flow in the mini-MFIT. Independent knowledge of the flow rate is crucial for sensor calibrations and development of high-fidelity flow measurements using electrochemical sensors. Pictured in Figure 6, the salt level sensor consisted of a continuity measurement device connected to an array of evenly spaced electrodes. As depicted in the diagram in Figure 6c, the level sensor measured the continuity between the salt tank and the four electrodes in the sensor. When the salt touched an electrode in the sensor, a circuit between the electrode and the salt tank was completed by the salt. The continuity measurement device measured the voltage generated by the small current (<1  $\mu$ A) which was allowed to flow between electrode and salt tank when the salt was touching the electrode. The continuity measurement sensor was powered by an Arduino Nano and custom code. It displayed the status of each electrode (submerged or not submerged) with indicator LEDs and could transmit the status of each electrode to a receiving computer via a USB cable. In Figure 7, a program was written for calculating and logging the flow rate. The salt level and fluid flow rate were measured by correlating the instant that the conductivity between each of the electrodes and the salt tank changes versus time.

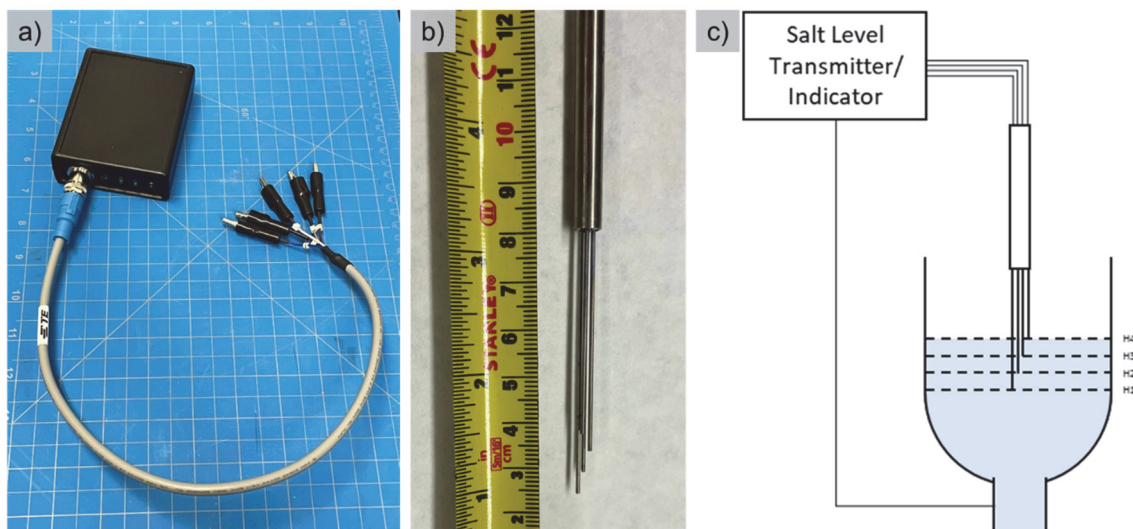


**Figure 6.** Mini-MFIT salt level sensor (a) continuity measurement device, (b) electrode array sensor, and (c) diagram of salt level sensor placement in the MINI-MFIT salt tank.

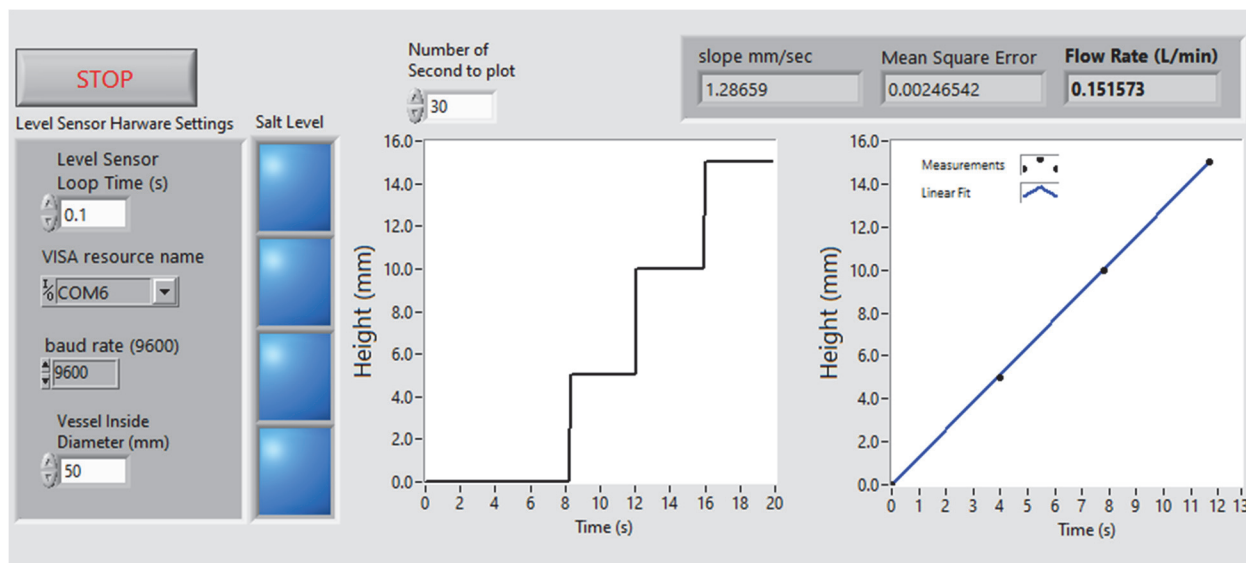


**Figure 7.** Mini-MFIT salt tank level sensor digital indicator software.

## 2.6 Software for Process Control and FEES Sensor Automation

In FY23, improvements were made to the MFIT process control software that enabled it to remotely control both the MFIT and the mini-MFIT. Figure 8 shows the MFIT control software during operation of the MFIT. A LabVIEW® module for plotting and logging process data, such as temperature, pressure, and process state, was implemented. This module enables additional interlocks that prevent the systems from reaching an unsafe condition. As shown in Figure 9, the software sequence programmer enables repeatable, high-throughput testing. This process automation greatly improved repeatability, throughput, and safety of experimentation.

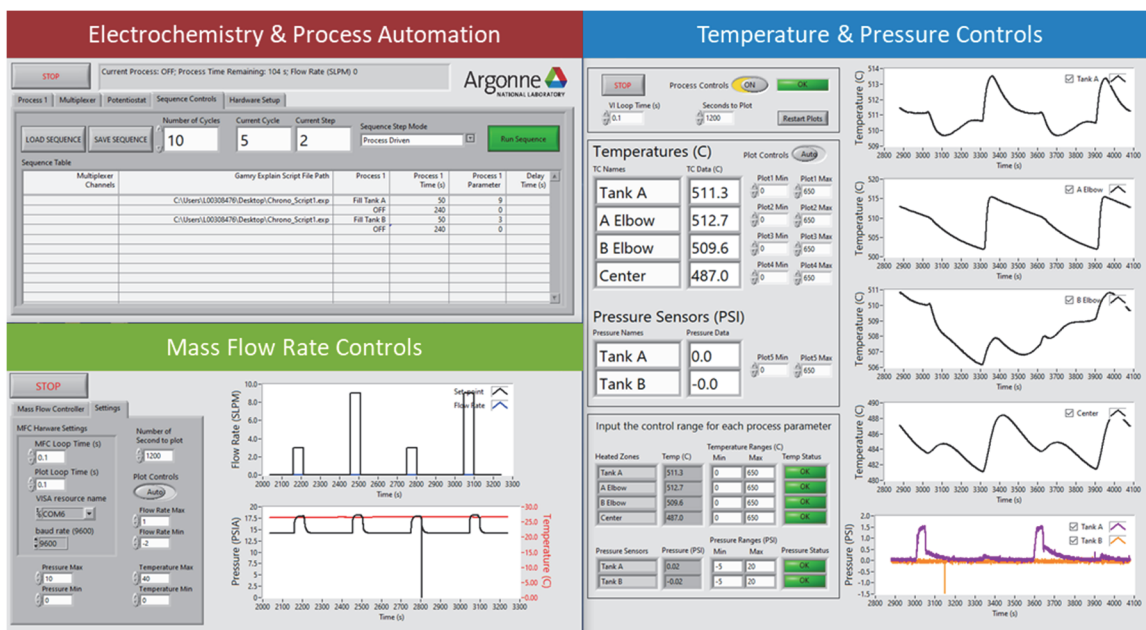


Figure 8. MFIT control software for process automation and FEES sensor control.

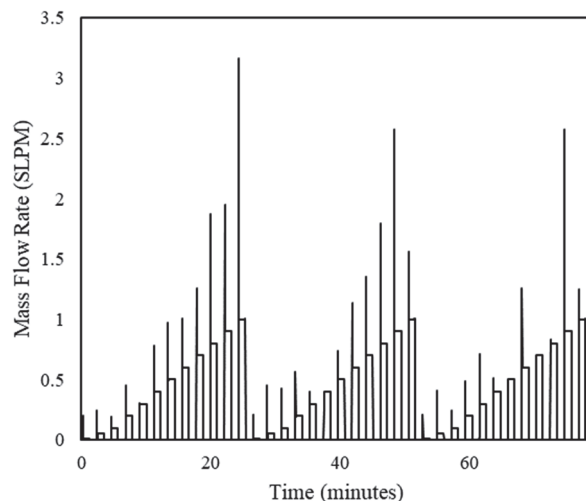
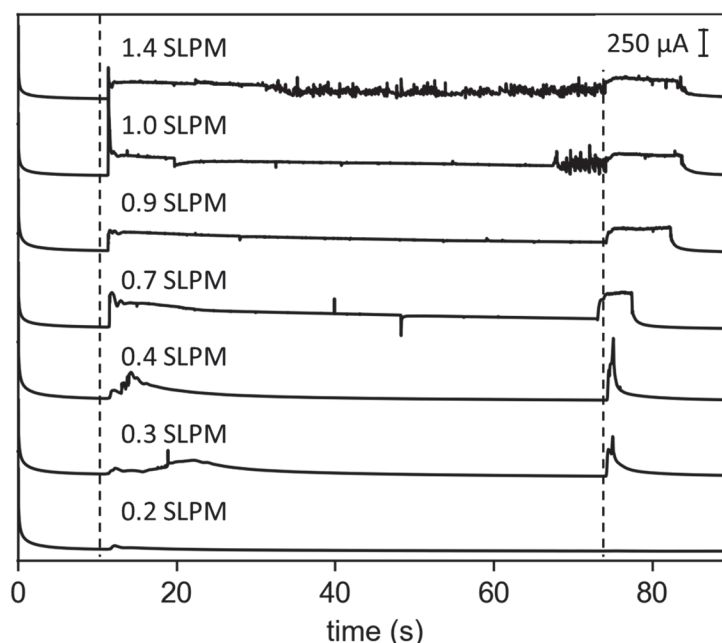


Figure 9. Mini-MFIT argon gas mass flow rate versus time for a repeated sequence of cycles at various set-points during testing in NaCl-KCl-MgCl<sub>2</sub> at 500 °C.

## 2.7 Mini-MFIT Shakedown Testing Using NaCl-KCl-MgCl<sub>2</sub> Salt

Mini-MFIT Shakedown testing was completed using NaCl-KCl-MgCl<sub>2</sub> salt to evaluate the feasibility of the furnace well-based design and gas control system. In Figure 10, constant potential measurements in flowing molten salt were taken over a range of mass flow controller setpoints between 0.2 and 1.4 SLPM. The first 10 seconds of the constant potential measurement correspond to a hold step in which no flow occurred. The fill step, denoted by the vertical dotted lines, was approximately 65 seconds long. Finally, the salt was allowed to drain freely from the mini-MFIT. The applied potential was 0.5 V vs. the W quasi-reference electrode. If impurities such as CrCl<sub>2</sub> are present, this is sufficient to induce a soluble-soluble oxidation reaction. The behavior of the current response over the range of flow rates is informative about the mini-MFIT's performance.





**Figure 10.** Mini-MFIT constant potential measurements during flow cycles at different mass flow controller setpoints in NaCl-KCl-MgCl<sub>2</sub> at 500 °C. The applied potential equals 0.5 V vs. W quasi-reference electrode.

At high flow rates the current response during the first few seconds of the fill cycle approached steady state consistent with findings from the larger MFIT system. At the highest flow rates, noise in the current response after several seconds of flow was caused by bubbling of argon gas up the dip tube after the salt in the crucible has been pulled into the MFIT.

Different trends in the constant potential current signal were observed at low flow rates that have important implications for mini-MFIT design of experiments. At relatively slow flow rates the rate of mass transport may be insufficient to supply a constant flux of species to the electrode. The current may decrease as the electrochemically active species are oxidized near the electrode surface. This was observed at mass flow controller setpoints around 0.7 SLPM. A critical mission of the mini-MFIT thus is to determine under what flow conditions the theoretical predictions can reasonably be applied.

When the setpoint was lowered below 0.7 SPLM a different behavior was present indicative of incomplete filling of the dip tube. The initial current response became increasingly delayed with slower setpoints. The behavior at setpoints below 0.7 SLPM is attributed to changes in FEES electrode submerged surface area as the horizontal section of the mini-MFIT dip tube fills with salt. It was clear that the validity of the constant potential measurement is dependent upon the FEES sensor being fully submerged in molten salt. Fortunately, the advanced MFIT control software and remotely operated gas control system enabled versatile multi-step cycles in which the dip tube can first be filled at a predetermined rate before switching to the desired setpoint for the constant potential measurement.

### 3. RESULTS

#### 3.1 Automated Transfers

During FY23, experiments were conducted to improve the performance of the sensors in simulated MSR conditions compared to earlier operations. The automation system enabled these types of tests and served to reduce the required user effort considerably. For example, using this system, a series of 80 transfers was completed early in FY23 to assess sensor performance over long durations. Similar tests had been run in FY22, but they were limited to only 5–10 transfers due to the need for manual operations. The results from the FY23 tests are shown in Figure 11. The transfers took place continuously over four days, and the average uranium concentration measured in the salt was  $1.642 \pm 0.008$  wt% over the duration of the transfer campaign. These transfers would have been very difficult or impossible without the addition of the automation system. As shown, the system worked consistently over the course of testing, thereby allowing us to take greater volumes of data throughout the year.

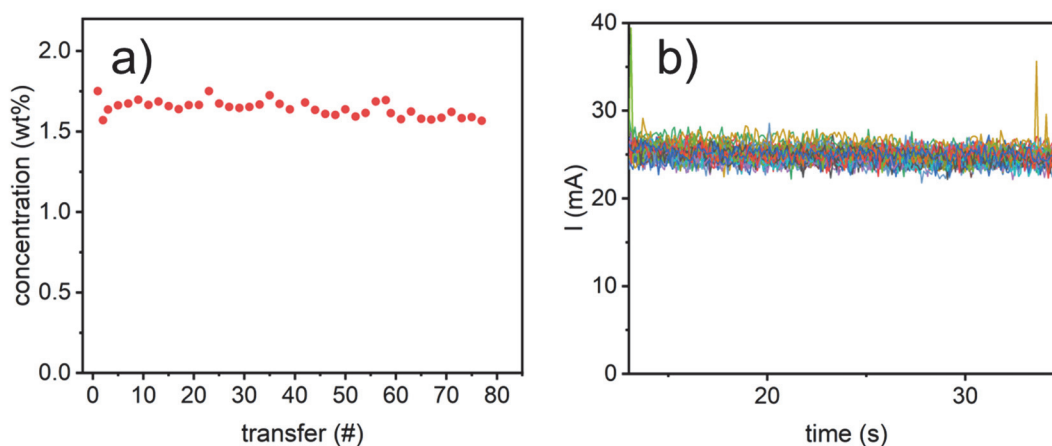


**Figure 11.** (a) Concentration calculation from FEES during 80 transfers at  $4.38 \pm 0.12$  L/min in  $\text{MgCl}_2$ -KCl-NaCl containing 2.0 wt%  $\text{UCl}_3$ . (b) Current response of FEES during 80 transfers.

#### 3.2 Sensor Assessment Campaign

With the automation system proven, we then sought to re-evaluate the performance of the FEES sensors across a wide range of actinide concentrations. Similar tests were performed in FY22, but oxygen ingressions served to increase the error to levels that were larger than anticipated. As described in Section 2.2, these tests consisted of  $\text{UCl}_3$  titrations from 0.5 wt% to 3.0 wt% to exercise the sensor across a wide range of loadings.

The testing campaign included operations of the stationary MAVS sensors along with operations of the in-flow FEES sensors. The MAVS was used to determine the concentration of  $\text{UCl}_3$  in the salt after each addition. Measurements were taken before and after transfers at each concentration and then averaged. A parity plot of the measured concentration versus process knowledge is shown in Figure 12. The relative standard deviation of these measurements was 2.6%.

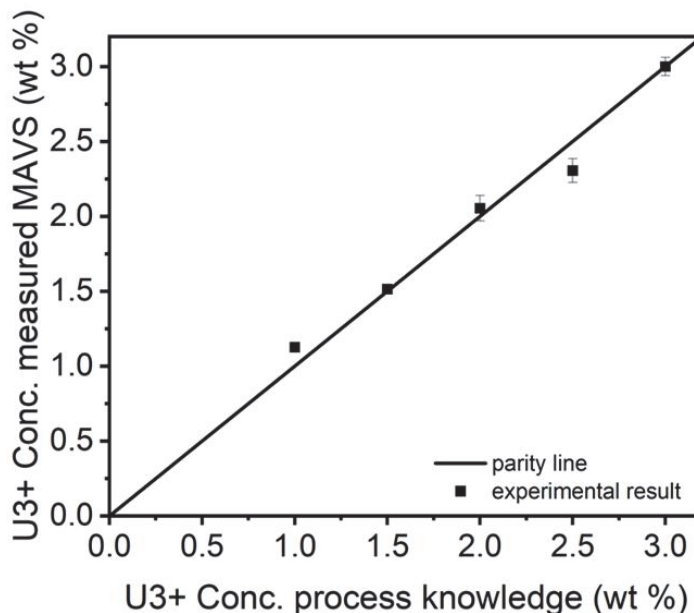


**Figure 12.** Concentration determined using stationary salt sensor in (MAVS) measured in  $\text{MgCl}_2\text{-KCl-NaCl-UCl}_3$ .

Flowing salt measurements were done throughout the titration campaign, and Figure 13 shows the current response associated with increases of the  $\text{UCl}_3$  concentration from 0 to 3 wt%. The response followed a linear pattern with an  $R^2$  value of 0.995. This indicated that the aliquots of  $\text{UCl}_3$  were consistent with each other and there was very little variance between additions. The graph shows improved consistency compared to FY22 data where  $R^2$  were typically  $\sim 0.977$ . This improvement resulted because of the increased number of runs per data point compared to FY22 as well as lower ingressions of air and water vapor into the system.

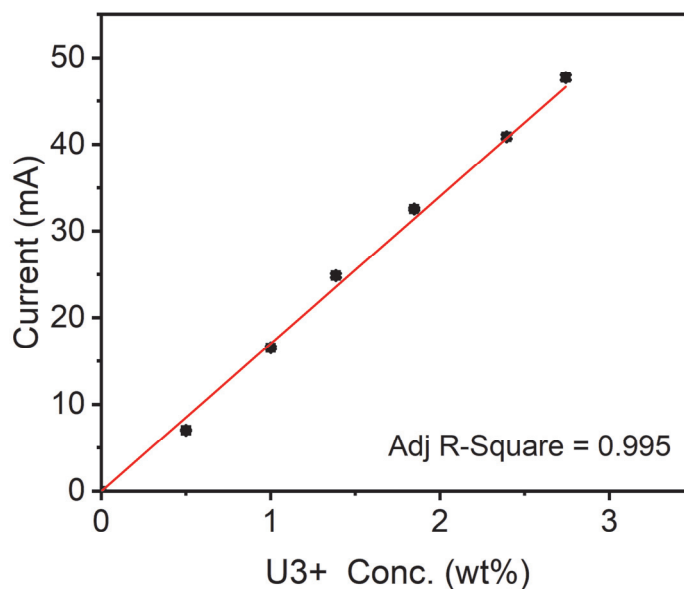


**Figure 13.** Current response of flow sensor at different  $\text{UCl}_3$  concentrations. Measurements were taken approximately 4.5 SLPM salt flow rate.

For each point, ten transfers were completed in FY23 vs. only three to four transfers in FY22. This was enabled by the retrofitting of automated valves and control software for the MFIT. Figure 14 shows typical results for the ten repeated transfers at the same concentration. The data was highly repeatable, as was observed last year. As a result of the increased number of runs, the relative standard error of the mean for representative measurements at a given concentration fell to 0.54% versus 0.97% in FY22. Measurements with abnormally high or low values did occasionally occur using the automation system. During these tests, which amounted to <10% of all measurements, large differences in the flow data and current response were observed. It is not clear what caused these occasional variations (possibly temporary clogging of issues with the gas delivery system), but these points were removed from the statistical analyses.

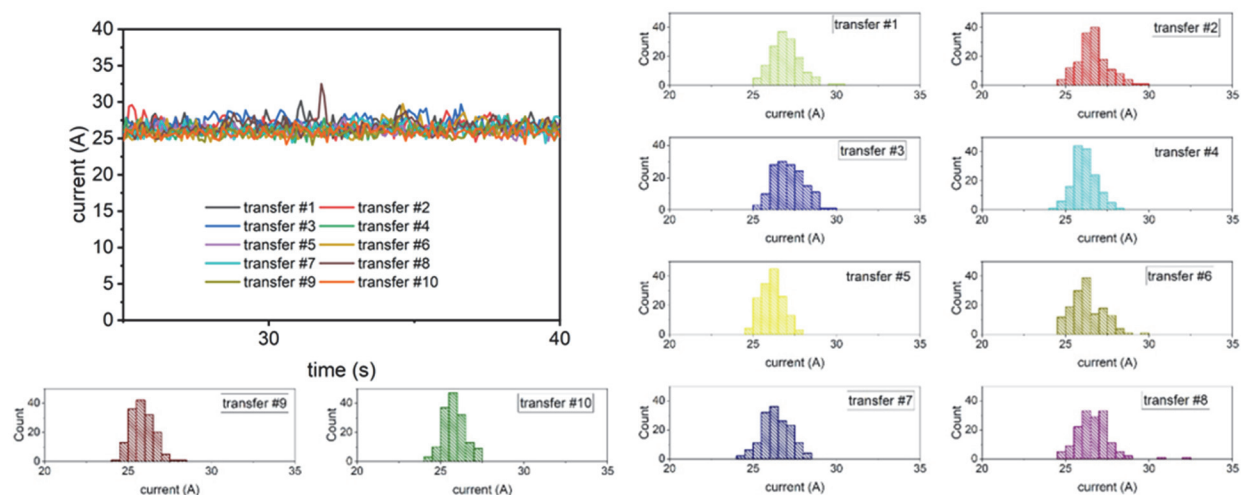


Figure 14.  $U^{3+}/U^{4+}$  current response and histograms of 10 repeat transfers using the FEES.

Table 2. Statistical properties of soluble/soluble current response during individual salt transfers (sampled at 10 Hz)

	Transfer #1	Transfer #3	Transfer #6	Transfer #9
Mean Current (mA)	26.96	27.14	26.30	25.83
Standard Deviation (mA)	0.87	0.91	0.95	0.66
Confidence Interval (99.0%) (mA)	0.182	0.192	0.199	0.139

Table 3. Statistical properties of soluble/soluble current response from repeated salt transfers (sampled at 10 Hz)

Metric	Value from Repeated Transfers
Mean Current (mA)	26.40
Relative Standard Deviation	0.54%
Confidence Level (99.0%) (mA)	0.370

Figure 15 shows the current response of the flow sensor to different flow rates across the full range of uranium concentrations. The data points are averages over ten transfers while the lines are a non-linear surface fit to the sensor response equation that was developed in FY22 (Equation 1).

$$i = \beta C Q^n \quad \text{Equation 1}$$

$$\beta = \frac{(\pi/4)^{1-m} d D_i z F k S c^{1/3}}{\rho} \left( \frac{\rho}{\mu d_0} \right)^m \quad \text{Equation 2}$$

Here,  $i$  is the current,  $\beta$  is an agglomerated Sherwood number pre-factor,  $C$  is the uranium concentration, and  $Q$  is the flow rate. In the definition of  $\beta$ ,  $D$  is the diffusion coefficient of the species of interest, and  $d$  is the relevant length scale (e.g., the diameter of the electrode),  $z$  is the number of electrons associated with the oxidation reaction,  $F$  is Faraday's constant,  $k$  is a Sherwood number pre-factor,  $Sc$  is the Schmidt number,  $\rho$  is the density, and  $\mu$  is the viscosity.

The fit of the sensor response function to the measured currents was generally good, although some deviation was present at low concentrations where the fit over-estimated the concentration of uranium in the salt. This discrepancy was also noted in FY22. The origin of these differences is unclear but is likely due to residual impurities in the salt reacting with the  $UCl_3$  as it is added and oxidizing it to  $UCl_4$  and to  $UO_2$  which then crashes out of solution and is not measured by the flow sensor. Both mechanisms are likely to be seen in a real flow loop if there is any ingress of oxygen or water into the loop. In the range of 1.0% to 3.0%, the agreement of the sensor response function improved greatly.

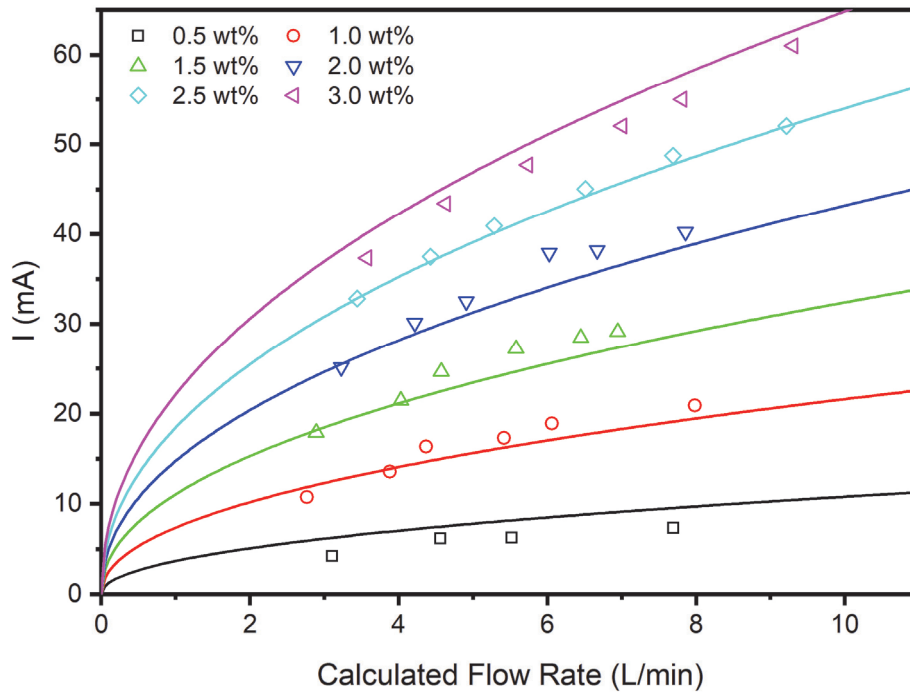


**Figure 15.** Experimentally measured current response of flow sensor at different  $U^{3+}$  concentrations and flow rates. Lines represent the nonlinear-surface fit for the sensor response function.

Figure 16 shows the parity plot of measured uranium concentration versus process knowledge using the sensor response function. The low-concentration predictions were underestimated, once again likely due to the oxidation of  $UCl_3$  affecting the response of the FEES sensor. Compared to FY22, however, the

measurements are significantly improved. Excluding the 0.5 wt% data that for both years showed large relative errors, a like-for-like comparison of data showed a mean absolute relative error of 3.1% in FY23 compared to 5.6% in FY22. This improvement was largely due to the repeatability of the measurements that was enabled by the automation system compared to manual operations. This level of error is still too large for mass accountancy purposes, but the continual improvements we have been able to show year-on-year suggest that error bounds approaching 1% may be possible in the future. Further enhancements to the performance are being explored with the mini-MFIT system, in particular improvements to uncertainty associated with the flow rate measurements which can impact the quality of the concentration measurements.

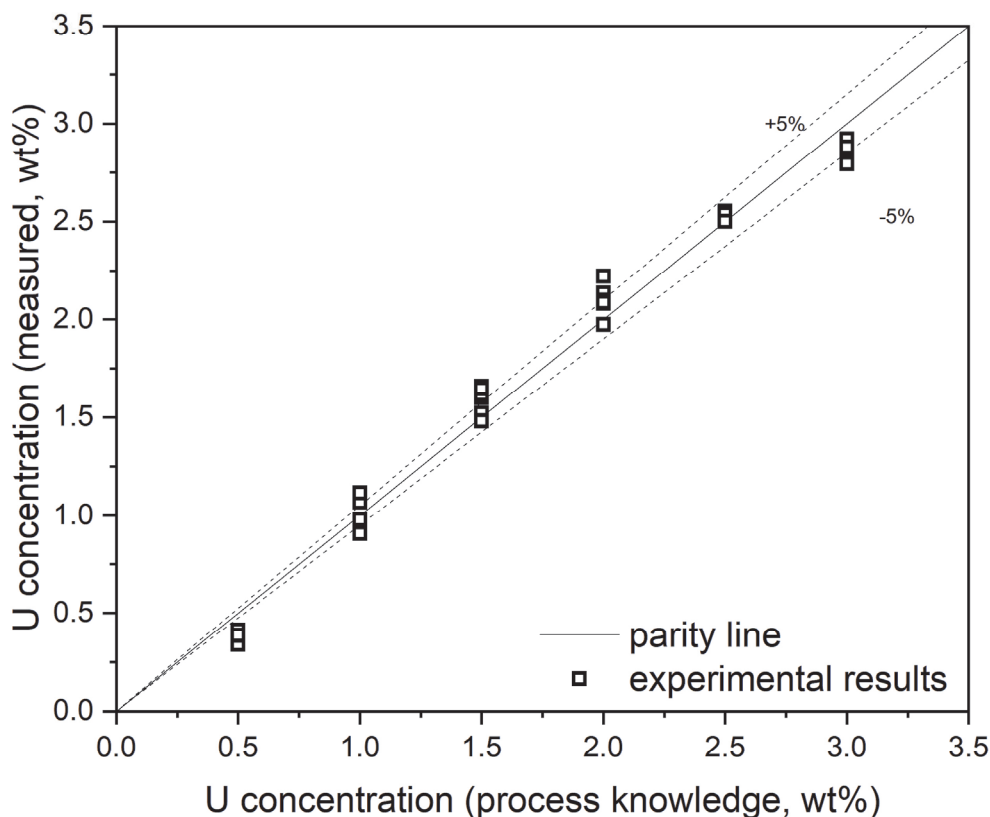
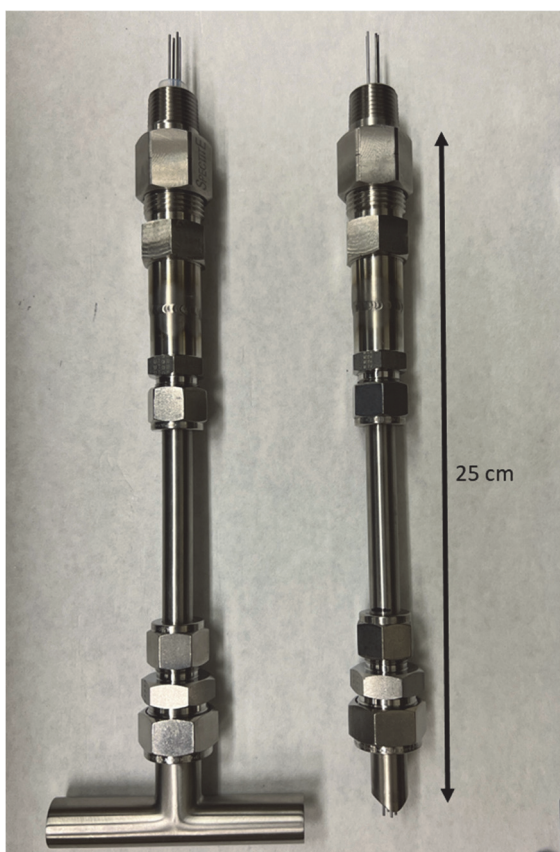


Figure 16. Parity plot of uranium concentration from process knowledge and uranium concentration measured using the FEES.

## 4. Engineering-Scale FEES Sensor Deployment

Beyond testing within the MFIT, in Q4 FY23, two FEES sensors (Figure 17) were deployed at an industrial partner's molten salt experimental facility to demonstrate chemistry and flow rate measurement capabilities at engineering scales. The general design of the FEES sensor was identical to the versions deployed in the MFITs, but upgrades were made to make the sensors compatible with fluoride salts and to improve sealing (given that the partner's flow system is not located in a glovebox). Improvements to the sensor's flow path were also pursued to ensure minimal disruption to the flow in the loop. Each FEES was inserted into a salt flow tube with an inside diameter of 16 mm. The two sensors have been installed at different points along the length of the same salt flow circuit enabling study of performance under similar flow conditions but different temperatures.

At present, the sensors have been fully installed into the flow loop and tested at temperature under pressurized argon gas. Photos of the installation of one such installed sensor is shown in Figure 18. Leak detection around the electrode feedthroughs showed no leaks, and the temperatures of the seals and compression fittings were well under their maximum limits. The sensors are planned to be evaluated in a 1000 hour flowing LiF-BeF<sub>2</sub> (66:34 mol. %) (FLiBe) test commencing in FY24 Q1.



**Figure 17.** FEES sensors deployed at industrial partner's engineering scale forced convection FLiBe experiment.



**Figure 18.** FEES sensor installed in industrial partner's flow loop

## 5. CONCLUSIONS

MFIT operations continued in FY23 resulting in improved performance of the FEES. The increased number of experimental runs and higher consistency of operations resulted in improved measurements. This work was enabled by the addition of an automation system for the operation of valves and salt transfers for the MFIT. This automation system monitored and recorded the thermocouple temperatures, tank pressures, and flow controller parameters, which were displayed for the user in a readable way. The software furthermore added capabilities to perform scripts for multiple transfers, with each transfer able to trigger electrochemical tests simultaneously. All these improvements allowed end users to make decisions about the conditions occurring within the MFIT flow system; these types of automated capabilities will also ultimately be crucial within full-scale MSRs.

The sensor campaign that occurred during FY23 showed significant improvements compared to FY22. For example, the mean absolute relative error of measurements across the range of uranium concentrations was 3.1% in FY23 compared to 5.6% in FY22. More improvements need to be made to reduce this to a level suitable for material accountancy, but in general, the updates to sensor design and operations that we have made so far indicate that the needed performance may be achievable. The main focus area for improvements at present is in regard to the determination of the salt flow rate. This flow rate ultimately controls the sensor response, and accurate values are required to ensure that the concentration measurements are accurate as well. Exploration of flow rate measurements will continue in FY24.

Alongside testing in the MFIT, our sensor and automation technologies have been deployed to a partner institution to provide an illustration of these tools' industrial relevance. These sensors have been installed and are being prepared for operations in a salt flow loop in early FY24. We believe that this testing campaign will appropriately demonstrate the high levels of accuracy, stability, and longevity that can be achieved using flow-enhanced electrochemical sensors combined with automated operations and analysis tools.



## REFERENCES

- [1] M.S. Greenwood, B. Betzler, “Modified Point-Kinetics Model for Neutron Precursors and Fission Product Behavior for Fluid-Fueled Molten Salt Reactors,” *Nuc. Sci. and Eng.* vol. 193, 417–430, 2019.
- [2] M.P. Dion, M.S. Greenwood, K.K. Hogue, S.E. O’Brien, L.M. Scott, G. Westphal, MC&A for MSRs: FY2021 Report, ORNL/SPR-2021/2305, 2021.
- [3] A.M. Lines, S.D. Branch, H.M. Felmy, J.M. Wilson, G.J. Lumetta, S.A. Bryan, “On-line monitoring combined with spectroelectrochemistry for the characterization of uranium and fission products within molten salt environments, PNNL-SA-144352, 2020.
- [4] J.A. Lubbers, “Raman Spectroscopy-Based In Situ Composition Monitoring System for Molten Salt Reactors”, 600-000-0622-00, 2019.
- [5] J. Guo, N.C. Hoyt, M. Williamson, “Multielectrode Array Sensors to Enable Long-Duration Corrosion Monitoring and Control of Concentrating Solar Power Systems,” *J. Electroanal. Chem.*, vol. 884, 115064, 2021.
- [6] S. Maji, S. Kumar, K. Sundararajan, “Exploring LIBS for Simultaneous Estimation of Sr, Ba And La in LiCl-KCl Salt,” *Optik*, 207, 163801 2020.
- [7] J.R. Cheatham III., A.T. Cisneros JR., J.F. Latkowski, J.M. Vollmer, C.J. Johns, “Fission reaction control in a molten salt reactor,” US10438705B2, 2019.
- [8] N.C. Hoyt, J.L. Willit, M.A. Williamson, “Communication—Quantitative Voltammetric Analysis of High Concentration Actinides in Molten Salts,” *J. Electrochem. Soc.* vol. 164, pp. H134–H136, 2017.